Numerical and Experimental Investigation of Flow Separation in Ovalized Nozzles

Sebastian Jack[†] and Chloé Génin[‡]

[†]German Aerospace Center, DLR, Institute of Aerodynamics and Flow Technology
Braunschweig, Germany, D-38108

[‡]German Aerospace Center, DLR, Institute for Space Propulsion
Lampoldshausen, Germany, D-74239

Abstract

During the unsteady start-up and shut-down process in supersonic rocket engine nozzles high sideloads can occur. Fluctuations, e.g. in the propellant feeding mass flow or the ambient pressure, can excite the nozzle's Eigenmodes leading to deformation and, in the worst case, to destruction of the nozzle structure. Separation of the nozzle flow amplifies this excitation. The flow characteristics in ovalized rocket nozzles and their influence on the nozzle structure is therefore investigated within the framework of the DLR internal cooperation program ProTAU. Three TIC nozzles have been designed, manufactured and tested to provide validation data for numerical simulations. The influence of the used turbulence model on the wall pressure and shock system have been investigated for the undeformed and a set of generically deformed nozzle contours.

NOMENCLATURE

β	nozzle contour wall angle
ε	area ratio: $(R_{exit}/R^*)^2$
a	amplitude
e	numerical eccentricity: $\sqrt{R_{max}^2-R_{min}^2}/R_{max}$
M	Mach number
R	radius

INDICES

$*$	nozzle throat
amb	ambient
def	deformation
des	design state
$exit$	exit plane
MD	Mach disc
sep	separation
tot	total

ABBREVIATIONS

NPR	nozzle pressure ratio: p_{tot}/p_{amb}
RSM	Reynolds stress turbulence model
SA	Spalart Allmaras turbulence model
TIC	truncated ideal contour

INTRODUCTION

Two general flow regimes occur during a rocket engine nozzles operation. While under steady flight conditions the supersonic flow inside the nozzle follows the contour, for very low nozzle pressure ratios (NPR) which appear during the unsteady start-up and shut-down phase, it separates from the wall. Downstream the separation line the wall pressure increases to the magnitude of the ambient pressure. An asymmetric separation line can therefore lead to high side loads. Asymmetric flucuations, caused by e.g. cumbustion instabilities or the instationary flow around the rockets body during the launchers ascent (buffeting), can excite the nozzles Eigenmodes leading to deformation and, in the worst case, to destruction of the nozzle structure. For a high NPR, when no separation occurs at the nozzle wall, the change in the wall pressure caused by deformation results in a force counteracting the local displacement. The interaction between flow and structure damps the systems excitation. In a separated nozzle flow a local outward deformation shifts the separation position in the upstream direction, increasing the local wall pressure, causing a further contour deformation. In this highly overexpanded case the difference between wall pressure in the nozzle and its ambience leads to an amplification of the local defor-

mation and therefore to an excitation of the system and an ovalized nozzle structure.
For a detailed description of the ovalization mechanism and side load generation in rocket nozzles see [1] [2] [3]. Since the first stage engine of current launcher systems has to perform well under a wide range of ambient conditions from sea-level to very low ambient pressure, their nozzle is usually designed to avoid flow separation and their aforementioned effects in the early flight phase. A better understanding of these processes could help improve the dimensioning of over-expanded rocket nozzles and thus the performance of future launcher systems. The flow characteristics in ovalized rocket nozzles and their influence on the nozzle structure is therefore investigated within the framework of the DLR internal cooperation program ProTAU.
Flow separation in deformed rocket nozzles has been investigated in different studies by various authors. For a literature overview see [1] [4]. Most of these studies were numerical simulations since the experimental measurement of the flow-structure-interaction in a supersonic nozzle is very challenging. In the present study, starting with rotation-symmetric geometries, the complexity of the deformation is therefore increased step by step to be able to investigate the underlying phenomena. In each phase - from steady state over flow response to a defined deformation to full flow-struture-coupling - numerical and experimental studies are carried out to collect validated data.

Nozzle Geometries

As a first step three undeformed nozzles were designed, as a basis for the deformation study. Truncated ideal contour (TIC) nozzles were chosen due to their relatively simple shock pattern which also influences the flow separation behaviour. For comparability all three geometries are designed to be full flowing at NPR 50 and have the same throat radius of R^*=10mm. The nozzles differ in their design Mach number and therefore their length, area ratio and exit wall angle. An overview of the design parameters is given in table 1.
To examine the effect of nozzle ovalization on the flow, a set of seven deformed geometries was created out of the three TIC nozzles by varying the amplitude, distribution and starting point of the deformation. While in realistic configurations the expected deformation amplitude is not bigger than three percent of the nozzle exit radius, it is varied from five to fifteen percent for the present study to ensure the ovalization effects are sufficiently measureable in the upcoming experiments. The cooling channels in the throat region of a rocket engine nozzle impose a thick and very stiff wall followed by a much thinner structure downstream the interface point which is usually located at an area ratio of five. The geometries were therefore deformed from an area ratio of five on to the nozzle end, except for geometry six which was deformed along its complete divergent part. Since in this first step the nozzle structures properties were not being of interest the deformation distribution was assumed to be a linear axial evolution for geometry five and a parabolic deformation for all other contours. Table 2 shows an overview of the deformation parameters of the generated geometries.

Name	M_{des}	β_{exit}	ε
TIC-48	4.8	5.0°	16.9
TIC-53	5.3	8.5°	18.5
TIC-58	5.8	11.3°	19.3

Table 1: Undeformed nozzle geometry parameters

Geometry	Base	a_{def}/R_{exit}	$\varepsilon_{def,start}$	Function
1	TIC-48	5%	5	parabola
2	TIC-48	10%	5	parabola
3	TIC-48	15%	5	parabola
4	TIC-53	10%	5	parabola
5	TIC-53	10%	5	linear
6	TIC-53	10%	1	parabola
7	TIC-58	10%	5	parabola

Table 2: Deformed nozzle geometry parameters

Experimental Setup

The three initial (rotation-symmetric) nozzles have been manufactured and tested under cold flow conditions. The three contours have been chosen to ensure full flowing condition at NPR 50. This value lies within the NPR limits obtainable under ambient conditions at test facility P6.2 at DLR in Lampoldshausen.

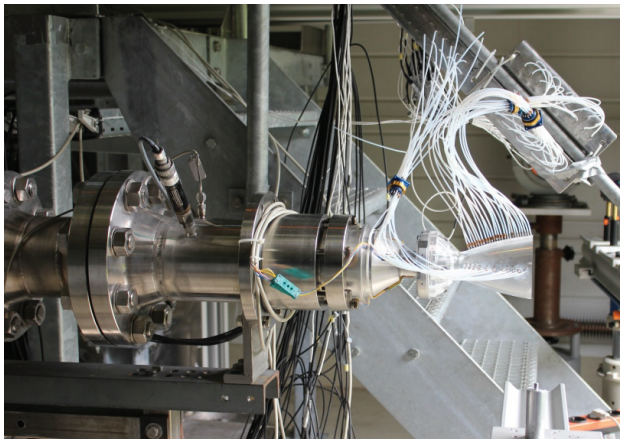

Figure 1: Nozzle equipped with sensor hardware on test bench P6.2

The test specimen were placed on the horizontal test rig and alimented with dry nitrogen. The flow turbulence was reduced by a combination of grids and a honey comb placed upstream of the nozzles convergent part. By regulating the nozzle feeding pressure, the NPR can be regulated following ramps of various gradients. A typical test featured a pressure variation with a low gradient (in the range of 1 to 2 $^{\mathrm{bar}}/_{\mathrm{s}}$), so that the flow condition can be considered as "quasi steady state". In addition, each test was repeated at least three times to verify the good reproducibility of the data.

The nozzle models were equipped with pressure transducers placed along the nozzle wall. The small interval between the pressure ports (4 mm) allowed following the flow separation position, from the throat to the nozzle end. The transducers used for this work were Kulite piezoresistive sensors. They were connected to the flow through a system of small pipes and Teflon tubes (see figure 1). Total conditions (pressure and temperature) were measured downstream the settling chamber. The measurements were realized with a 1 kHz scan rate and filtered with a low pass 160 Hz filter.

The evolution of the flow patterns was also recorded with schlieren optics. A black and white Z-setup has been used to visualize the shock system outside the nozzle. The pictures were recorded during up- and down-ramping with 2000 frames per second. For the optical investigation, the feeding pressure ramp was set to 20 $^{\mathrm{bar}}/_{\mathrm{s}}$ to limit the total amount of pictures.

CFD

Numerical Method

All presented simulations were performed using the DLR finite-volume solver TAU. The stationary Reynolds averaged Navier-Stokes equations were solved using either the Spalart Allmaras (SA) or a Reynolds stress (RSM) turbulence model to close the turbulent equations. In comparison to other turbulence models based on the Boussinesq approximation the original formulation of the SA performs reasonably well for separated supersonic nozzle flows [5]. Since anisotropic effects are neglected when using the SA model a RSM model was used for comparison. Nitrogen, treated as perfect gas, was chosen as fluid model. The calculations have been carried out on hybrid grids of either a quarter section ($90°$ opening angle) with symmetry planes or a full model of the respective geometry. Automatic mesh adaptation was used to ensure grid convergence. An example of the experimental and simulated wall pressure distribution as well as a schlieren image compared to the density gradient magnitude in the results of a SA simulation for nozzle TIC-53 at a NPR of 40 is shown in figure 2.

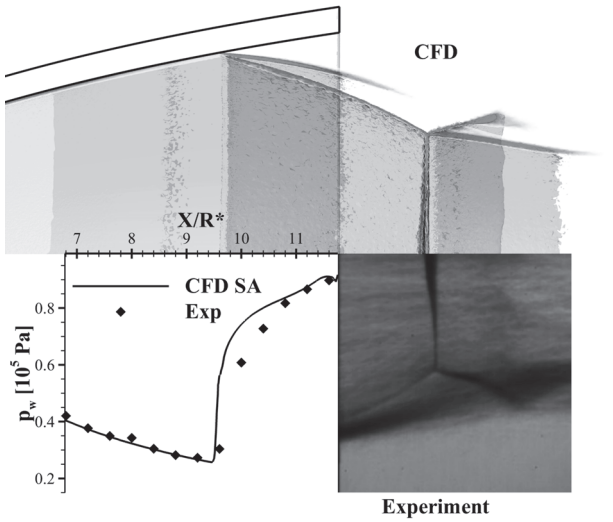

Figure 2: Comparison between CFD and experiment for TIC-53, NPR 40

Undeformed Nozzles

Figure 3 shows the wall pressure distribution calculated by the CFD solver in comparison to those measured in the experiment for the three undeformed nozzle geometries. Regarding the separation position, the difference between the results computed with the SA one equation turbulence model and the experimental data lies within the accuracy of the measurement for NPR $\geq$ 35. There are two major effects that cause the deviation to increase with decreasing NPR which have been observed in earlier studies as well [5] [6]. Due to these effects, the resulting shock and separation positions are dependent on the size and shape of the recirculation area. First of all the pressure gradient along the separation shock is calculated steeper than it is measured in the tests. Additionally the static pressure in the recirculation area downstream the shock position is underestimated. The flow around the sharp edge at the nozzle end produces a vortex in the SA simulation that leads to a local pressure maximum that was not observed as strong in the experimental data.

For comparison the TIC-53 nozzle has also been simulated using a RSM turbulence model, since this model is capable to model the anisotropy of the turbulence in this subsonic regime of the nozzle flow. The effect of both of the aforementioned mechanisms on the wall pressure distribution was significantly lower in the RSM simulations. In contrast to the results of the SA simulation the static pressure in the recirculation area, as well as its gradient along the separation shock, is in good agreement with the experimental results. Furthermore the pressure in the vortex near the nozzles exit plane is calculated correctly. Since the RSM model seems to have the tendency to overestimate the separation position, its difference to the experimental

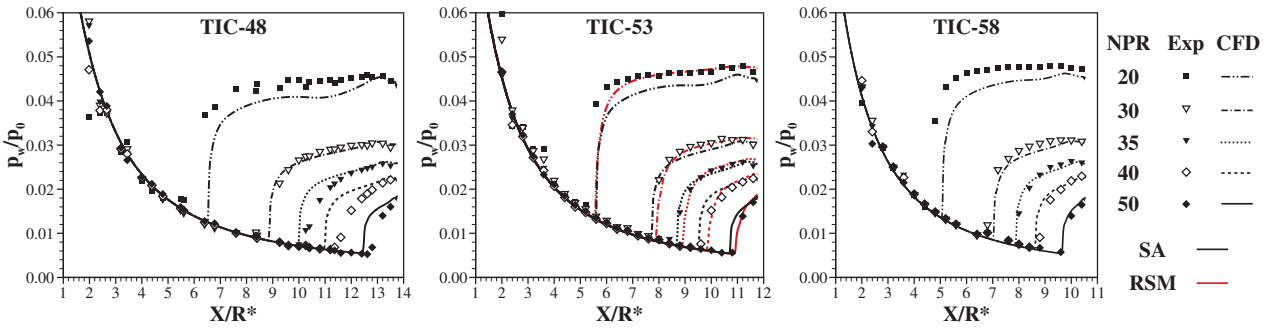

Figure 3: Calculated and measured wall pressure

values is in the same order of magnitude as in the SA simulations. The deviation is however relatively independent of the NPR.

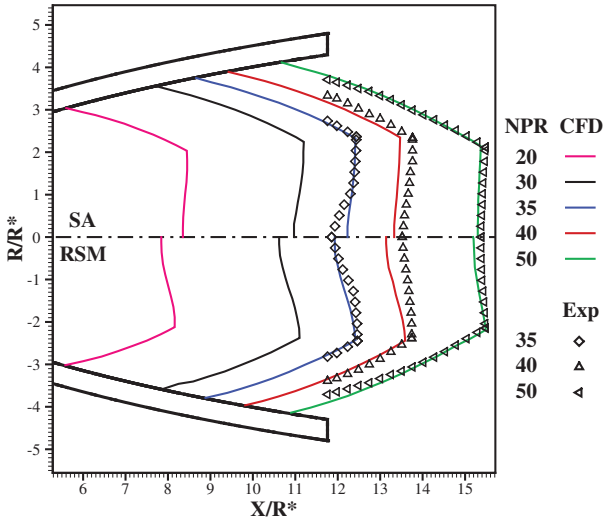

Figure 4: Shock geometry comparison between CFD and experiment

Figure 4 shows the shock geometry in the nozzle TIC-53 as calculated by the CFD solver and measured in the experiments by Schlieren images. The position of the triple point, where the oblique separation shock and the Mach disc meet, is well predicted by the simulations using the SA and the RSM model. While the angle and position of the separation shock show only slight differences, the shape of the Mach disc is affected by the used turbulence model. Both simulations, as well as the experimental data, show the strongest bending of the Mach disc for a NPR around 35. For this pressure ratio the Mach disc is located around the point where the flow near the symmetry axis of the nozzle reaches its design value and aligns parallel to the axis. This behaviour is in good agreeement with earlier studies and theoretical investigations based on inviscid calculations performed by Nasuti et. al. published in [7]. While in the SA simulations the curvature of the bended Mach disc is underpredicted, it is considerably stronger pronounced when using the RSM model. This difference is increasing with decreasing NPR and therefore bigger recirculation zones and a vortex dominated flow in the end section of the nozzle. Due to the fact that the experimental shock positions are obtained from optical measurements, no data for these conditions is available, since in this case the shock system is positioned completely inside the nozzle. The simulation results are in good agreement with the experimental data and the applied method can therefore be considered validated.

Deformed Nozzles

To measure and visualize the effects of the deformation parameters on the flow characteristics the separation line and the Mach disc were automatically extracted from the flow field data and appropriate functions were fitted to their geometries. The post-processing software tecplot 360 was used to calculate the separation line using its correspondent function which is based on the MIT FX library [8]. The distorted sine function equation (1) was fitted to the resulting raw data.

$$X = a_{sep} \cdot sin\left(2\varphi + \Delta\varphi + c \cdot sin\left(2\left(\varphi - \frac{\pi}{2}\right)\right)\right) + \bar{X}_{sep} \quad (1)$$

To detect the Mach disc and quantify its curvature the local maxima of the pressure gradient magnitude has been analyzed. In the cross section a hyperbolic paraboloid, in the radial section another sine function were fitted to the obtained data. Equations (2) and (3) show the functions used to describe the saddle shaped Mach disc. All fits were calculated using the least square method. Figure 5 shows a typical flow pattern and the fitted functions. For information on how the deformation itself effects the parameters of the fitted functions see [1].

$$X_{MD} = a_{MD} \cdot sin\,(2\varphi + \Delta\varphi) + \bar{X}_{MD} \tag{2}$$

$$1 = \left(\frac{Z_{MD}}{R_{MD,max}}\right)^2 + \left(\frac{Y_{MD}}{R_{MD,min}}\right)^2 \tag{3}$$

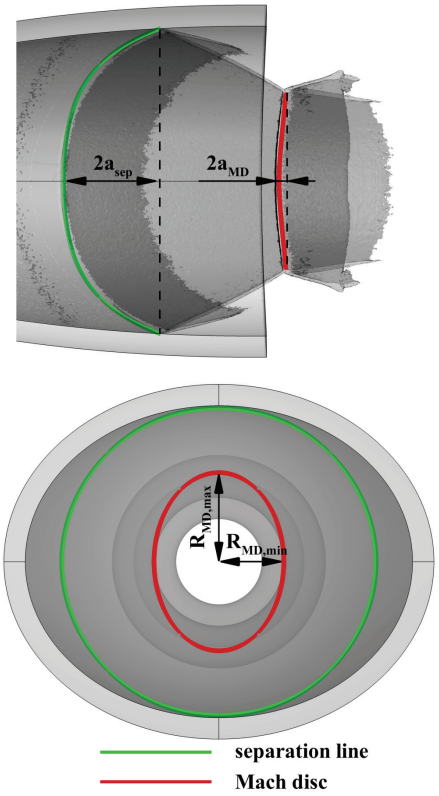

Figure 5: Mach disc (red) and separation line (green) for geometry 2 and NPR 35

To investigate the influence of the used turbulence model and computational domain simulations on quarter section grids and grids of the complete nozzle (designated by their corresponding opening angle of $90°$ and $360°$) were performed.
Although in the results for the rotation-symmetric nozzles the used turbulence model had a significant effect on the flow in the recirculation area and the separation position, it only caused a difference of approximately 2.5% in the separation fit amplitude a_{sep}. As already indicated by the results presented for the undeformed nozzles, the deformation of the Mach disc was dependent on the turbulence model. Figure 6 shows the amplitude of the fitted sine function over the nozzle pressure ratio. The RSM model predicted a stronger deformation of the Mach disc in axial direction than those in the SA simulations.
A similar tendency could be observed in the numerical eccentricity of the Mach disc border e shown in figure 7. The effects of the deformation onto the

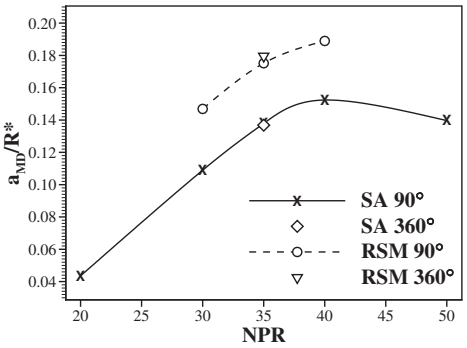

Figure 6: Amplitude of Mach disc sine fit

shock structure were emphasized when using the RSM model compared to the SA reference case.
The comparison of the exemplary full geometry simulations in figures 6 and 7 show that the used symmetry planes in the quarter section model had no measureable influence in the shown instationary simulations.

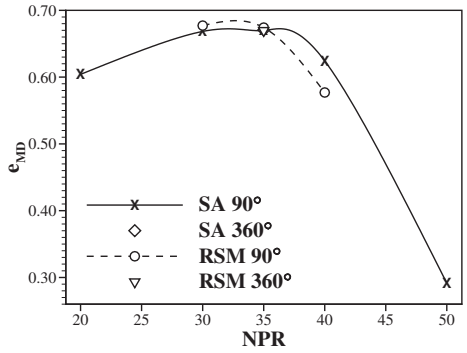

Figure 7: Numerical eccentricity of Mach disc border ellipse fit

Conclusion

In a first step of the current investigation of the supersonic flow in ovalized nozzles a set of undeformed geometries was created to validate the numerical method and study the underlying phenomena. Validation data was provided by pressure measurements and Schlieren images of cold flow tests.
While the Spalart Allmaras turbulence model yields to a fast and reliable prediction of the separation position of the nozzle flow, it shows small but systematic differences in the calculated wall pressure distribution compared to the experimental data. Since the wall pressure difference between the flow inside the nozzle and its ambience leads to the self amplifying structural effect of nozzle ovalization, these deviations may become of interest in the further investigation of the deformed geometries. By the use of a Reynolds Stress turbulence

model the shock pattern, as well as the flow in the recirculation area of the nozzle and the corresponding wall pressure distribution, were simulated more accurate and did fit the experimental data. Although the SA model can provide a first approximation, the use of a high order turbulence model is therefore advised for detailed investigation of pressure induced forces that deform the nozzle structure. An exemplary comparison for a deformed geometry confirmed the aforementioned for the influence of the deformation on the flow characteristics as well.

For the subsequent step of the presented study on ovalization three deformed geometries have been manufatured as stiff models and will again be tested under cold gas condition at DLR Lampoldshausen. The provided data will be used to validate the presented simulations.

REFERENCES

[1] C. Génin, R. Stark, and S. Jack. Flow Separation in Out-of-Round Nozzles, a Numerical and Experimental Study. In *5th European Conference for Aerospace Sciences (EUCASS)*, 2013.

[2] T. Damgaard, J. Östlund, and M. Frey. Side-Load Phenomena in Highly Overexpanded Rocket Nozzles. *Journal of Propulsion and Power*, 20(4):695–704, 2004.

[3] J. Östlund. Flow Processes in Rocket Engine Nozzles with Focus on Flow Separation and Side-Loads. 2002.

[4] A. Hadjadj and M. Onofri. Nozzle Flow Separation. *Shock Waves*, 19(3):163–169, 2009.

[5] R. Stark and G. Hagemann. Current Status of Numerical Flow Prediction for Separated Nozzle Flows. In *2nd European Conference for Aerospace Sciences (EUCASS)*, 2007.

[6] B. Wagner, S. Karl, and G. Hagemann. Test Case 1a: Short Nozzle Under Separated Flow Condition, a Numerical Investigation with the DLR TAU-Code. In *FSCD-ATAC Workshop*, 2006.

[7] F. Nasuti, M. Onofri, and E. Pietrapaoli. Prediction of Shock Generated Vortices in Rocket Nozzles. In *43rd AIAA Aerospace Sciences Meeting and Exhibit*, 2005.

[8] B. Haimes. FX – Fluid feature eXtraction tool-kit. http://raphael.mit.edu/fx, 2014. Online, accessed 25-April-2014.